Comparison of Diurnal Warming Estimates from Unpumped Argo Data and SEVIRI Satellite Observations

Sandra L. Castro[a*], Gary A. Wick[b], and Justin J. H. Buck[c]

[a] Colorado Center for Astrodynamics Research, University of Colorado, Boulder, CO, USA

[b] NOAA/Earth System Research Laboratory/Physical Sciences Division, Boulder, CO, USA

[c] British Oceanographic Data Centre, Liverpool, UK

*Corresponding author. University of Colorado, CCAR 431 UCB, Boulder, CO 80309, USA.

e-mail address: sandrac@colorado.edu

Tel: +1 (303) 4921241

Fax: +1 (303) 4922825

For Submission to: Remote Sensing of Environment

March 29, 2013

Abstract

Estimates of diurnal warming at the ocean surface from modified Argo floats providing unpumped measurements of temperature up to the surface are compared against collocated satellite-derived values from the Spinning Enhanced Visible and Infrared Imager (SEVIRI) flying on the METEOSAT-9 Second Generation (MSG) geostationary satellite. The amplitude of diurnal warming is computed from the difference between subskin and foundation temperature estimates derived independently from the Argo and SEVIRI data. The results demonstrate remarkable consistency between the observations, lending support for both products and the associated methodologies, particularly for estimation of the foundation temperature. Individual subskin values agree to within an absolute mean difference of ≤ 0.1 K and standard deviations of the differences are < 0.4 K. Statistics for comparison of the foundation temperatures are similar. Differences between the corresponding derived estimates of diurnal warming have negligible bias and standard deviations < 0.25 K. The strong agreement of the diurnal warming estimates exists even when excluding nearly isothermal profiles, suggesting the differences are robust to small spatial offsets and point-to-pixel differences. The results particularly support the ability of the modified Argo floats to provide reliable, and highly valuable, measurements of the near-surface temperature, helping to argue for more modified floats. Moreover, the results suggest that the unpumped Argo data has the potential to provide an independent estimate of the foundation temperature for validation of SST analyses. The method for estimating the foundation temperature from SEVIRI represents a good compromise between data coverage and influences of cloud contamination and nighttime cooling.

1. Introduction

The diurnal cycle of the sea surface temperature (SST) is the result of the interplay among solar heating, turbulent mixing, and the dynamics of the heat exchange between the ocean and the atmosphere. Under clear skies and low wind conditions, the absorption of incoming shortwave solar radiation rises the temperature of the water closest to the surface and a strong near-surface temperature gradient may develop during the day. At night, mixing by oceanic convection typically erodes the diurnal thermocline and the warm layer disappears/decays due to evaporative cooling and the absence of incoming solar radiation. Cooling progresses until sunrise, when the daily cycle of solar radiation may lead to the formation of a new warm layer atop the previous night's convective mixed layer, if light wind conditions persist. Because the absorption of solar heating is strongest at the surface, the greatest rises in temperature are confined to shallower layers closer to the surface (at depths of ~0.5–1 m). Wind mixing, however, can transport the absorbed heat downwards, and deeper, more moderate warm layers can be found in the upper 10–20 m of the surface.

The strength of this diurnal warming amplitude is regulated by cloud cover, which modulates insolation, and wind stirring, which influences turbulence mixing. If the wind is sufficiently calm and there is strong insolation, the warming at the ocean surface sensed by satellites can be highly significant. In situ observations from moorings have shown warming in excess of 5ºC at depths of 0.3–0.6 m (Flament et al., 1994), also evident in coincident thermal infrared (IR), 1-km AVHRR imagery. Although the surface signature of diurnal warming events as seen from satellites vary significantly in extent and with geographic region, often times they are shaped into long narrow streaks with embedded blobs/patches of extreme warming. Flament et al. (1994) documented coherent streaks of warm temperature off the California Coast from

AVHRR IR imagery, typically ~50–100 km long and ~4–8 km wide, with patches of extreme warming of up to 6.6ºC. Extreme diurnal amplitudes exceeding 4 K have also been reported by Stramma et al. (1986) and Ramp et al. (1991). Recently, satellite observations from multiple sensors have observed streaks with patches of extreme warming up to 7 K in magnitude (Gentemann et al., 2008), and there is a consensus now within the SST community that these patches of extreme warming are not artifacts of the SST retrieval. Average amplitudes for diurnal warming events, however, are typically smaller, on the order of tenths of a degree (e.g., Stuart-Menteth et al., 2003), and extend over wide horizontal areas in excess of 100 000 km^2. It has been suggested that warm streaks have preferential locations following high atmospheric pressure ridges, typically associated with light surface winds and clear skies (e.g., Deschamps and Frouin, 1984; Cornillon and Stramma, 1985; Stramma et al., 1986). Despite the apparent good correlation between synoptic atmospheric pressure fields and the spatial extent of warming features seen from space, modulation of diurnal warming amplitudes at smaller scales is not well understood.

Diurnal variability in the SST is significant for multiple applications ranging from production of daily SST analyses to studies of low-frequency weather and climate variability. Present satellite-derived SST analyses attempt to blend data from multiple sensors with different measurement times and different effective measurement depths. To create a blended SST product representative of a specific time and depth or a daily value representative of a depth free from any diurnal warming influence (the foundation temperature, see e.g. Donlon et al., 2007), it is necessary to compensate for the different amounts of diurnal warming present in each satellite retrieval. Beyond removing diurnal variations for daily SST analyses, capturing the diurnal variability in SST is important for accurately estimating the air-sea heat flux. Multiple

investigators have demonstrated the impact of diurnal temperature variations on the time integrated heat flux over limited periods and regions (e.g., Fairall et al., 1996; Schiller and Godfrey, 2005; Danabasoglu et al., 2006). Recently, Clayson and Bogdanoff (2013) showed that diurnal variations can result in yearly average flux differences of up to 10 W m^2 over significant portions of the tropical oceans. Furthermore, accounting for diurnal warming has been shown to improve Madden-Julian oscillation predictability (Woolnough et al., 2007) and to affect simulated amplitudes of the El Niño-Southern Oscillation (ENSO) (Ham et al., 2010; Masson et al., 2011).

Because of its impact, substantial efforts have been applied to estimating diurnal warming amounts with models and satellite-derived products. A dedicated diurnal warming model was developed by Fairall et al. (1996) for application to air-sea interaction studies and later enhanced by Gentemann et al. (2009). Detailed physical models have also been evaluated and applied to the generation of larger scale maps of diurnal warming (e.g., Pimentel et al., 2008; Horrocks et al., 2003; Wick et al., 2002). Other models have been developed specifically for integration into weather and climate models (Zeng and Beljaars, 2005; Schiller and Godfrey, 2005). Additional simplified parameterizations have been developed both from observations (Gentemann et al., 2003; Stuart-Menteth et al., 2005; Filipiak et al., 2010) and from more detailed physical models (e.g., Webster et al., 1996; Kawai and Kawamura, 2003) for easier application to satellite observations. Initial climatologies of diurnal warming have been developed based on both satellite observations (Stuart-Menteth et al., 2003) and model calculations (e.g., Clayson and Weitlich, 2007; Bellenger and Duvel, 2009).

There is an important need for more direct observations of diurnal warming of the sea surface to support these efforts. Detailed uncertainty estimates for modeled diurnal warming and

retrieved amplitudes from geostationary satellites are notably absent, particularly for the more extreme amplitude events. Existing observations from research ships and moorings are very limited, particularly given the depth of the measurement, the low frequency of occurrence of the large events and their spatial extent.

Argo floats (Roemmich et al., 2001) present a unique opportunity for measuring the warming of the near-surface layer of the ocean due to their high-resolution sampling capabilities in the upper meters of the ocean. These floats collect regular profiles of temperature and salinity from mid-ocean depth to the surface using sensors with stringent accuracy requirements for climate research. The present array is comprised of over 3,000 floats well distributed throughout the globe. Typical Argo floats profile about once every 10 days and surface at times distributed nearly uniformly throughout the diurnal cycle. The main issue, however, is that sampling is normally halted at a depth of about 5 m below the surface to prevent biofouling of the sensors in the uppermost layer of the ocean. This means that, under the conventional modus operandi, Argo floats may fail to detect the peak diurnal warming amplitude, and particularly, the most extreme warming events corresponding to shallower heated layers trapped right beneath the surface.

A specific subset of Argo floats (APEX Argo floats) that enable sampling the temperature right up to the surface have been deployed by the United Kingdom, United States, Japan, and India since 2008. These floats collect unpumped temperature measurements in addition to the standard pumped measurements. Work at the University of Washington (Anderson and Riser, 2012) and the United Kingdom Met Office (Carse et al., 2012) has demonstrated the ability of these floats to capture realistic profiles for a number of cases of significant diurnal warming at the ocean surface. The absolute accuracy and stability of the

unpumped temperature measurements and derived diurnal warming amplitudes, however, is not well known.

This paper further evaluates the utility of these unpumped Argo temperature measurements to provide accurate measurements of the near-surface temperature (NST) and diurnal warming. The observations are compared against satellite-derived measurements from the Spinning Enhanced Visible and Infrared Imager (SEVIRI) flying on the METEOSAT-9 Second Generation (MSG) geostationary satellite. The work cannot be considered a pure validation of the Argo measurements as both datasets have uncertainties in their observations. Instead, this paper examines the consistency between the observations that would lend support to the quality of both datasets. The question of unpumped Argo data quality is of significance to the Diurnal Variability Working Group (DVWG) of the Group for High Resolution Sea Surface Temperature (GHRSST) as these floats may provide valuable direct in situ measurements of diurnal warming, and a completely independent validation data set for satellite SST analyses. It would also aid in ongoing interactions with the Argo community as the relative merit of pursuing additional enhanced floats or changes to the standard operating procedures are being explored. The work also enables an assessment of the consistency of foundation temperature estimates from both Argo and SEVIRI. The significance of this foundation temperature is further established in the following section.

2. Data/Methods

2.1. Terminology

It is useful to first establish some key terminology used in this work. GHRSST defined (Donlon et al., 2007) terms for several specific temperature values in the near-surface layer of

the ocean. The “skin” SST refers to the temperature of a layer down to approximately 10-µm depth as would be measured by an IR radiometer. This is the closest measurement to the actual “interface” temperature that can be practically obtained with present sensors. Within the skin layer, which has negligible heat storage capacity, heat transfer occurs by molecular conduction. Because the neat heat flux at the surface is nearly always from the ocean to the atmosphere, the oceanic skin layer is typically cooler than the water below by ~ 0.2 K (see e.g., Saunders, 1967). The temperature directly beneath this skin layer is referred to as the “subskin” SST. Estimates of the subskin SST are commonly provided by microwave radiometers or, indirectly, from IR satellite radiometers referenced to subsurface measurements such as from drifting buoys or moorings. Temperatures at other depths are referred to as SST-at-depth and the effective depth should be specified.

The concept of the “foundation” temperature was introduced to facilitate discussions of diurnal warming and analyzed SST products. The foundation temperature is defined as the temperature at the base of the layer influenced by diurnal fluctuations in SST. It is important to emphasize that it is a theoretical concept, and as such, there is no direct measurement of the foundation temperature. While it is commonly approximated by quantities such as the pre-dawn value of the temperature between 1–5 m depth, the foundation temperature should not be associated with a specific depth; instead, it should be thought of as the temperature closest to the surface at which diurnal warming effects are negligible. Validation of daily SST analyses that seek to provide a foundation temperature estimate are particularly problematic. There is interest in determining if Argo temperature profiles can provide a potentially viable independent estimate of the foundation temperature from the observed temperature at the base of the diurnal thermocline.

The diurnal warming estimates in this work will be computed as differences between a subskin SST and an estimate of the foundation temperature. When continuous time series of the surface temperature are available, it is possible to estimate the diurnal warming amplitude from its evolution throughout the solar cycle. For Argo profiles at discrete times, however, it is necessary to estimate the amplitude from the profile itself. For the SEVIRI data, an estimate of the foundation temperature will be derived from the available sequence of satellite scenes as described below.

2.2. Unpumped Argo data

Near surface temperature profiles from specialized APEX Argo floats with unpumped temperature measurements were obtained from the British Oceanographic Data Centre (BODC). The data set contains both pumped and umpumped measurements supplied at depths of approximately 5, 10, 15, and 20 dbars. The conductivity, temperature, and depth (CTD) pump is then turned off at ~5 dbars, and unpumped temperature and pressure are measured every 6 seconds up to the surface. Data collected between January 2009 and March 2012 were utilized in the study. Because of the geographic coverage of SEVIRI (60N–60S, 70W–45E), only those floats deployed in the Atlantic Ocean were considered.

Argo float surfacing times were supplied by BODC and were estimated using the time for start of transmission, which is known to the second minus 12 minutes, as defined by the International Argo Data Management Team (ADMT). The method is described in http://www.argodatamgt.org/content/download/5261/38297/file/Method-Position-Time-QC.pdf). The offset of 12 minutes is based on known float behavior and allows the finishing of piston movements and preparation of data for satellite transmission.

APEX Argo floats measure surface pressure offset at the start of the float cycle just before descent to park approximately 9–10 days before the profile is made. This is transmitted by the float and used to correct the pressure data for sensor drift (Baker et al., 2011). Surface pressure offsets were supplied directly by the BODC.

The APEX near surface temperature firmware collects samples from the pressure and temperature sensors through the sea surface producing a time series that includes subsurface measurements and samples measured after the sensor has breached the sea surface. Samples taken above the sea surface are removed assuming samples every 0.6 dbars (~10 s) in the top 5 m. A pressure differential (Δp) between two consecutive measurements < 0.5 dbar is considered as an indication that the float has reached the surface since it indicates the float ascent rate has dropped below the nominal ascent rate of 0.09 ± 0.03 dbar/s (see Johnson et al., 2007, for details on ascent rates). This method may filter out some good data when there are strong density gradients near the surface that slow the float ascent. It does, however, minimize sampling when the sensor is clear of the sea surface.

Values extracted from the Argo profiles included the shallowest standard pumped measurements (at ~5 dbar) and estimates of the subskin and foundation temperature from the unpumped data. The subskin and foundation temperature were both determined manually from visual inspection of the NST profiles. A sample profile from the unpumped data for a case with significant diurnal warming is shown in Figure 1 along with the identified subskin and foundation temperature estimates. The subskin SST was taken as the peak temperature value approaching the surface. For cases where sharp cooling was observed on top of the warm layer, as in the profile shown in Figure 1, the peak value below this cooling was used. It is possible that the cooling occurs after the temperature probe breaks the surface and is exposed to the air. It

is not believed that the current Argo temperature probes can reliably resolve cooling across the skin layer of the ocean due to their response times (0.6 s). The foundation temperature is taken as the temperature at the shallowest depth in the profile before warming near the surface is observed visually. The onset of warming is fairly obvious in the example in Figure 1, but there will clearly be some uncertainty in the foundation estimate in general. Any warming extending to depths below the deepest available measurement of 20 m would not be detected. Diurnal warming (DW) is then computed as the difference between the subskin and foundation temperature estimates (DW = SST subskin – SST foundation). The shallowest pumped temperature measurement (typically at a depth of ~5 m) is also extracted for comparison of results available using standard Argo floats and data reporting. No use of the pressure data is made other than estimating the time when the float breaks the surface, thereby eliminating it as a source of uncertainty.

2.3. SEVIRI SST Retrievals

The SST retrievals from SEVIRI were derived operationally by the European Organisation for the Exploitation of Meteorological Satellites (EUMETSAT) Ocean and Sea Ice Science Application Facility (OSI-SAF) at Météo-France/Centre de Météorologie Spatiale (CMS) in Lannion, France, and obtained through the archive at the French Research Institute for the Exploitation of the Sea (IFREMER). The retrievals are generated using a non-linear SST (NLSST) type approach (e.g., Walton et al., 1998) with coefficients derived from radiative transfer models to which a numerical weather prediction (NWP) model based correction is applied (Le Borgne et al., 2011; 2012). While the SEVIRI measurements are inherently of the skin temperature, the values are adjusted to nighttime buoy measurements during the retrieval

252 (Le Borgne et al., 2012) and, hence, will be treated as subskin SSTs in this analysis. The data are
253 available hourly at 0.05° resolution, but, for ease in data access, we used 3-hourly gridded data at
254 0.1° resolution constructed from the highest quality hourly data. Sampling from the MSG
255 satellite provides coverage of much of the Atlantic Ocean and Mediterranean Sea. For the period
256 of 2009–2012, the data came from the SEVIRI on METEOSAT-9.

257 The quality of SST retrievals from SEVIRI is generally perceived to be very good.
258 Estimates of diurnal warming from SEVIRI have been shown to be consistent with those derived
259 from other satellites (Gentemann et al., 2008), and in agreement with measurements from
260 drifting buoys (Le Borgne et al., 2012). Comparison against retrievals from geostationary
261 satellites is best for diurnal warming studies because of the continuous sampling throughout the
262 diurnal cycle, enabling a greater number of collocations than with polar orbiting satellites. Other
263 geostationary satellites like previous GOES have experienced complications with their
264 calibration, which hinder accurate retrieval of diurnal variations (Wick et al., 2002; Yu et al.,
265 2013). For this reason, the analysis was limited to SEVIRI retrievals.

266 Subskin and foundation temperature estimates for comparison with Argo are derived
267 from the available SEVIRI SST retrievals. Values are obtained both from the pixel containing
268 the location of the Argo profile, and from an average of the cloud-free retrievals in the 5x5 pixel
269 array centered on that pixel. The subskin estimate is taken from the retrieved SST in the scene
270 closest in time to the surfacing of the float. As a result, the maximum allowed time difference
271 between the Argo profile and SEVIRI subskin measurements is 1.5 hours. The foundation
272 temperature estimate is derived from a composite of the preceding nighttime SEVIRI SST scenes
273 to enable better cloud-free coverage than would be available from a single pre-dawn scene.
274 Cloud-free retrievals collected between 2200 local solar time (LST) and 0700 LST are averaged

together to form the composite. An example of the SEVIRI foundation temperature estimate for January 28th 2012 and the corresponding climatological foundation map for January, are shown in Figure 2. The individual foundation estimate, unfortunately, still has significant gaps even after averaging the multiple nighttime scenes, but the values appear reasonable with respect to the climatology.

As with other GHRSST products, proximity confidence maps, with values ranging in a scale of 1–5, are provided with each SEVIRI SST image. Proximity confidence values are defined based on the most likely sources of error for each satellite sensor, and left at the discretion of the satellite data producer. For this analysis, all retrievals with proximity confidence values provided were considered. Those retrievals judged as confidently cloudy are not included in the SST product. Values were not limited to the "best" quality values (3–5) as this resulted in a very limited number of collocations, but more importantly, by discarding pixels with degraded confidence in the proximity of clouds, many cases of perfectly valid diurnal warming, as corroborated by the Argo, were being eliminated. For some other GHRSST products excluding other than the "best" values has also been observed to result in the elimination of valid instances of diurnal warming.

2.4. Data Collocation

The location of the Argo observations, collocated with SEVIRI, is shown in Figure 3. The background images correspond to 3-month, maximum value composites of DW peak amplitudes (computed as the difference between SEVIRI SSTs from 1200–1500 and 0000–0300 LST) observed during the study period. Matches are shown here only when valid cloud-free SEVIRI subskin and foundation estimates are both available for a coincident Argo profile, so

298 that diurnal warming can be estimated from the satellite. No restrictions were imposed on the
299 percentage of available cloud-free pixels in the 5x5 subarray. The spatial distribution of the
300 collocations is clearly limited by the deployment locations of the specialized APEX Argo floats.
301 Matches occurred largely along the South Atlantic Current with a few cases in the North
302 Equatorial Current. The most extreme warming events in the SEVIRI data tend to occur during
303 the summer months (June-July-August (JJA) for the Northern Hemisphere and December-
304 January-February (DJF) for the Southern Hemisphere).

305 To facilitate the later analyses, the Argo temperature profiles were divided into two
306 categories: those exhibiting significant temperature gradients near the surface (cases with
307 warming), and those that were largely isothermal (cases with no warming). The two subsets are
308 reflected by the different colors in Figure 3, with black circles for the isothermal profiles and
309 magenta circles for profiles with identifiable diurnal thermoclines. The distribution of profiles
310 with warming is not significantly different from the overall distribution of matches.

311

312 **3. Results**

313 Before looking at the DW results, it is instructive to first compare the individual Argo
314 and SEVIRI estimates of both the subskin and foundation temperatures. Scatter plots illustrating
315 the relationship between the Argo- and the satellite-derived temperatures (based on the SEVIRI
316 5x5 pixel averages), are shown in Figure 4. Corresponding statistics are presented in Table 1.
317 The comparisons with the nearest SEVIRI pixel are very similar and, therefore, are not included.
318 Results are shown separately both for the subskin (Figure 4a) and the foundation (Figure 4b)
319 temperatures. Red and blue symbols correspond to Argo profiles with and without warming,
320 respectively. Statistics here include cases where the Argo floats were collocated with either the

SEVIRI subskin or foundation retrievals (coincident matches are not required). The overall agreement is found to be remarkably good for both the subskin and foundation estimates. The subskin values agree to within an absolute mean difference of < 0.1 K and standard deviations of the differences are < 0.4 K. The biases (computed as SEVIRI subskin SST – Argo subskin SST) are consistent (both in sign and magnitude) with those observed by Le Borgne et al. (2012) for SEVIRI retrievals relative to drifting buoys, but the standard deviation values are even smaller (by ~0.2 K). Perhaps some improvement could be attributed to better quality of the temperature sensors on Argo floats (the temperature accuracy requirement for sensors on Argo floats is 0.005 K, whereas the typical accuracy of those deployed in drifting buoys is 0.1 K). The averaging of SEVIRI data over 3 hours could also reduce noise and point-to-pixel differences. In any event, the positive results lend confidence to the quality of the subskin estimates from both SEVIRI and Argo. Moreover, the fact that the statistics are similar for the more complex warming cases as for the isothermal cases supports the ability of the unpumped Argo CTD sensors to provide accurate measurements of diurnal warming. Finally, the quality of the statistics relative to the previous drifting buoy comparisons (Le Borgne et al., 2012) also suggests that the ascent time of the Argo floats is being reasonably estimated, at least for comparison with a 3-hourly product.

The statistics for the foundation temperature estimates are also quite similar to those for the subskin values. While correspondence might be expected for the isothermal profiles, the excellent agreement for the cases with visible warming is all the more remarkable given the challenges in identifying the foundation and the inherent subjectivity of the manual identification method used here. This supports the methodology for estimating the foundation temperature in both products and, quite significantly, suggests that the Argo NST data has the potential to provide an independent estimate of the foundation temperature for validation of SST analyses.

The overall negative biases are consistent both with the subskin results and with Le Borgne et al. (2012). For those cases where warming is observed, the foundation bias is less negative than for the isothermal cases (–0.02 K vs. –0.11 K) meaning that the satellite foundation estimate is relatively warmer in comparison to Argo. This could be consistent with the SEVIRI foundation approach, based on a nighttime average, being elevated when surface cooling is still occurring through the course of the night. Interestingly, even though the foundation product is derived from multiple SEVIRI scenes, there are about the same number of matchups for the foundation comparisons as there are for the subskin, which corresponds to a single satellite scene. This could indicate a greater amount of data rejection in the nighttime SEVIRI SST retrievals due to cloud contamination.

To further illustrate the merit of the additional unpumped Argo NST measurements relative to the standard Argo pumped measurements, the SEVIRI SST values were also compared against the 5 dbar pumped temperature (Argo T5m). These values correspond to the best estimate of the near-surface temperature that would be available from traditional Argo floats. The statistics with respect to the Argo pumped temperature at 5 dbar are included in Table 1 along with the unpumped results. While the statistics are similar, as expected, for the isothermal cases, significant differences are observed when diurnal warming is present. The Argo T5m is 0.23 K cooler on average than the SEVIRI subskin retrievals and the standard deviation is increased by 0.05 K relative to the comparison against the unpumped value. Clearly, when diurnal warming is present, the shallowest Argo pumped measurement is not the best representation of the subskin temperature and the supplemental unpumped NST data provides valuable additional information. Comparing against the foundation temperature when diurnal warming is present, the Argo T5m is 0.16 K warmer on average than the SEVIRI foundation,

367 although the standard deviations are the same. The similarity of the statistics to the isothermal
368 cases suggests the Argo T5m may be more akin to the foundation temperature, but the fact that
369 the bias of –0.16 K is the largest negative difference encountered, implies the Argo T5m is still
370 likely overestimating the foundation temperature due to the presence of diurnal warming at 5-m
371 depth.

372 Given the favorable comparisons between the individual subskin and foundation
373 temperature estimates from Argo and SEVIRI, we next compared diurnal warming estimates
374 derived from the two products when collocations were available simultaneously for both the
375 corresponding subskin and foundation temperatures. The resulting scatterplot and corresponding
376 statistics are shown in Table 2 and Figure 5, respectively. The data points shown in Figure 5 are
377 only for those cases where warming was observed in the Argo profiles. While the individual
378 points show some notable differences, the results generally demonstrate good consistency
379 between the diurnal warming estimates from both products. The bias and standard deviation of
380 the residual difference between the SEVIRI- and the unpumped Argo-based diurnal warming
381 estimates (ΔDW = SEVIRI DW – Argo DW) are both very small (see Table 2). Interestingly,
382 though the scatter in the DW estimates in Figure 5 is clearly significant relative to the individual
383 mean DW amounts, the standard deviation of the difference (8^{th} column in Table 2) is slightly
384 more than half the standard deviation of the subskin and foundation residuals (4^{th} and 9^{th}
385 columns in Table 1, respectively).

386 The better agreement of the DW estimates implies that differences between the
387 corresponding subskin and foundation temperatures from SEVIRI and Argo are correlated, as
388 illustrated in Figure 6; i.e., differences in the estimated subskin SSTs vary in tandem with
389 differences in the foundation, for both warming and isothermal cases. Thus, where the SEVIRI

390 subskin retrieval is high relative to the Argo-derived estimate, the SEVIRI foundation estimate is
391 also likely high relative to the Argo foundation estimate. While there is increased variability in
392 the absolute DW estimates from SEVIRI and Argo, likely due to differences in measurement
393 location, time, and point-to-pixel inequalities (the satellite DW is a spatial average, whereas the
394 Argo DW is for a singular point), the corresponding diurnal warming estimates have less
395 variability. This is surprising given the "streaky" nature of peak diurnal warming, where spatial
396 variations in DW can be significant.

397 Additionally, it is worth noting from Table 2 that, when the Argo profiles are isothermal,
398 the SEVIRI DW estimates also suggest negligible mean (0.02 K) diurnal warming. This result
399 provides additional support for the foundation estimation method used with SEVIRI. We also
400 explored an alternate foundation methodology based on the minimum value composite of
401 nighttime SEVIRI retrievals, but this approach suggested an increase mean diurnal warming (0.2
402 K) for the SEVIRI estimate when compared against the isothermal profiles, due likely to residual
403 cloud contamination in the foundation product. Figure 7 shows the fractional cloud cover,
404 present in the nighttime mean-value composites, over the SEVIRI domain during the study
405 period. As can be seen from this figure, the Argo profiles used in the DW comparisons tended to
406 surface in areas of persistent cloudiness. Additional tests were performed restricting the
407 minimum value composite calculations to pixels with proximity confidence 3 or higher in order
408 to minimize the effect of cloud contamination in the alternate foundation methodology, but an
409 increased mean diurnal warming (0.1 K) was still observed for the isothermal comparisons.

410 The largest warming event captured in the matchup dataset has a moderate (but
411 significant) amplitude of ~2 K. While the maximum value composites in Figure 3 indicate that
412 DW events with amplitudes of up to 4.8 K were detected by SEVIRI during the 3 year span of

this study, none of these events, nor the more extreme ones noted by Gentemann et al. 2008, were sampled with the APEX Argo floats. Additional collocations for larger amplitude diurnal warming events are highly desirable to verify that the agreement observed here persists over the entire range of potential diurnal warming amplitudes.

A line of best fit (not shown) for the scatter plot on Figure 5, suggests a slight tendency for the SEVIRI-derived DW amplitudes to underestimate those from Argo, especially for the larger amplitude events. Differences of this sign are less problematic than they would be for the alternative, at least with respect to usability of the Argo NST data in estimating DW. An underestimate from the Argo measurements might suggest an inability of the unpumped Argo data to capture the peak warming occurring just beneath the ocean surface (such as due to inadequate flow past the sensor or inadequate sampling rates). Relative underestimates from SEVIRI can potentially be explained by multiple factors. It is possible that the saturation in the satellite estimates is the result of differences in effective spatial sampling scales. Gentemann et al. (2008), for instance, demonstrated that the perceived amount of warming was typically less for satellite products with coarser spatial resolution due to the localized nature of peak warming. A simpler explanation would follow from the fact that overestimating the satellite foundation can lead to an underestimation of the warming retrieved from the satellite. As discussed in connection with Table 1, the satellite-derived foundation temperature can be overestimated when averaging all the preceding nighttime observations in periods of greater diurnal warming. The calm wind condition required for the more severe warming events also produces the largest cool skin effects (e.g., see Figure 4 in Castro et al., 2012). Alternative methods explored here and designed to produce cooler foundation temperatures (e.g., minimum value composites of nightly scenes), however, produced poorer results.

A comparison of the residual differences between the DW estimates from SEVIRI and Argo (ΔDW) stratified by differences in the subskin (ΔSST subskin = SEVIRI subskin SST – Argo subskin SST) and the foundation temperature estimates (ΔSST foundation = SEVIRI foundation SST – Argo foundation SST) is shown in Figure 8. In this plot the circles represent the biases and the error bars represent ±1 standard deviation of the observed DW differences for each bin of the stratification variable. Since the ΔSSTs are highly correlated with each other as shown in Figure 6, the change in sign of the slope between Figures 8a and 8b follows from the definition of DW. As expected, the relationship shown is of no consequence for the isothermal cases; however, the bin plot suggests a clear linear dependence of the differences in DW from the satellite and Argo on the "misestimation" of the individual subskin and foundation SSTs for cases with DW. Assuming that incorrect SST estimates are attributable to either misinterpreting the Argo NST profiles or miscalculating the satellite foundation temperature, it is possible to speculate about the consequences these "errors" have on the DW estimates. From Figure 8b it follows that, in spite of the correlation between the subskin and foundation temperature differences, an overestimation of the SEVIRI foundation results in an underestimation of the warming retrieved from the satellite. Underestimating the foundation, however, appears to have a lesser impact on the satellite-derived warming as indicated by the slightly smaller bias and standard deviation of the red curve in Figure 8b. The sensitivity of the DW estimates to warmer SEVIRI foundations not only is consistent with the statistics described in Table 1, but also points to the importance of getting the satellite foundation estimate right. While this is a difficult task given the lack of consensus in the definition of the foundation itself, the overall agreement in the results of this work are quite positive.

458 A miscalculation in the subskin SST, on the other hand, is more likely to occur when
459 misinterpreting the peak warming in the Argo profile. Apart from the obvious (underestimating
460 the Argo subskin results in less warming retrieved from the float, which in turn introduces a
461 positive bias in ΔDW), what Figure 8a seems to indicate is that underestimating the Argo peak
462 warming has a more severe impact than overestimating it. This is confirmed by using Argo T5m
463 in the calculations of Table 2. An overestimation of the Argo foundation, by say using Argo
464 T5m as foundation, introduces a bias of 0.13 K in ΔDW (the statistics in Table 2 show zero bias
465 and a standard deviation of 25 K for the calculations using the APEX unpumped subskin SST),
466 although standard deviation is unaffected by this substitution. An underestimation of the Argo
467 subskin SST, also from using Argo T5m as proxy for the subskin, not only doubles the mean bias
468 of the DW residual (0.28 K), but also allows for almost twice as much variability relative to
469 previous case (0.39 K vs. 0.25K). This has important implications when looking at pressure to
470 determine the Argo subskin SST, as this method is more likely to underestimate the magnitude of
471 the subskin. As explained before, denser stratification (steeper diurnal thermoclines) will slow
472 down the float, and the temperature at $\Delta p < 0.5$ dbar will likely miss the peak of diurnal
473 warming. The uncertainty introduced by this method would need to be quantified, since the
474 pressure criterion is an easy alternative to automate the DW estimate from Argo floats. For this
475 work we did not use the Δp criterion, as we defined the Argo subskin SST visually from the NST
476 profile.
477 Finally, the residual differences between the warming estimates were compared with
478 other parameters including the time of day, matchup time difference, wind speed, shortwave
479 solar irradiance (derived from the 0.6 μm visible channel of SEVIRI), clear sky coverage, and
480 data quality to see if there were any systematic differences between the SEVIRI and Argo

481 estimates responsible for the scatter in DW. In particular, we explored the sensitivity of the DW
482 statistics to the clear sky coverage as discussed in Le Borgne et al. (2012). For this analysis, we
483 looked at the whole range of ΔDW values and divided them into 5 bins based on the percentage
484 of clear sky pixels in the 5x5 DW imagettes. These results are shown in Table 3 for cases with
485 and without warming, and all data combined. As this table indicates, there is no significant
486 difference in the ΔDW statistics, whether only those matchups with 100% clear sky are used in
487 the comparisons or if no distinction is made at all. No other clear dependencies were observed
488 for any of the remaining parameters considered.
489
490 **4. Conclusions**
491 Estimates of the subskin and foundation temperatures and corresponding diurnal warming
492 from SEVIRI satellite-based retrievals and special unpumped Argo measurements were
493 compared. The results demonstrate remarkable consistency between the products lending
494 support for both products and the associated methodologies. Given there are uncertainties in
495 both products, this work cannot be considered formal validation of either and cannot establish
496 definitive accuracy estimates. Nevertheless, the work represents an important step in
497 establishing the utility of both products.
498 Agreement was observed in both the individual subskin and foundation temperatures and
499 the corresponding derived diurnal warming. Correlation between differences in the subskin and
500 foundation temperature estimates from SEVIRI and Argo actually resulted in a smaller standard
501 deviation for the difference in derived diurnal warming than for the individual temperature
502 products. Thus, while the “streaky” and highly scale dependent nature of diurnal warming
503 events can complicate the comparison of diurnal warming amplitudes from different sensors, the

agreement here was found to be more robust to small spatial offsets and point-to-pixel differences than for the absolute temperatures.

The suggestion of the ability of unpumped Argo data to provide accurate estimates of diurnal warming is particularly significant. The potential utility of the Argo data has been a key question facing the GHRSST Diurnal Variability Working Group. Well-distributed independent measurements of diurnal warming, needed for validation of models and diurnal corrections, have been seriously lacking. The results further support, but go beyond previous studies demonstrating that, even in a normal operating mode, Argo floats do sample diurnal warming events of significance. Taken together, the findings strengthen arguments for the need of more modified APEX Argo floats capable of providing near-surface temperature measurements. Inclusion of the unpumped data with measurements at depths shallower than 5 m is seen to be critical for obtaining estimates of the peak diurnal warming occurring near the ocean surface.

The results have further implications for the operation and analysis of near-surface profile data from the Argo floats. The agreement demonstrates that issues regarding proper estimation of float ascent times are being handled well. The results also suggest that with complete temperature profile data from the upper ~20 m of the ocean it is possible to derive a meaningful estimate of the foundation temperature from the Argo data. Significant additional work is required to establish the validity of the foundation data, but these results are very encouraging.

Likewise, the results further support the utility of diurnal warming estimates from SEVIRI. Most difficult from SEVIRI is obtaining an estimate of the foundation temperature from which diurnal warming can be derived. The method based on averaging valid cloud-free observations from the preceding night was found to be a good compromise. Attempts to utilize

minimum values in the SEVIRI retrievals introduced likely residual cloud contamination, while use of only predawn values yielded too few collocations for meaningful comparisons.

Significant diurnal warming was again observed from SEVIRI, but the comparisons with Argo only captured events with amplitudes up to ~2 K. The agreement between the SEVIRI- and Argo-based diurnal warming estimates tends to further support the validity of the large diurnal warming amplitudes observed with SEVIRI, but direct validation of these events remains desirable.

Acknowledgements

Funding for this work was provided by the Multi-sensor Improved Sea-Surface Temperature (MISST) for IOOS. We thank Dr. Andrea Kaiser-Weiss for initiating a dialog between GHRSST and the Argo community about the potential use of NST Argo data in studies of diurnal warming.

References

Anderson, J. E., & Riser, S. (2012). Near-surface observations of temperature and salinity from profiling floats: The diurnal cycle, precipitation, and mixing, Abstract OS12C-03 presented at the *2012 Fall Meeting AGU*, San Francisco, Calif., 3–7 Dec.

Baker, P. M., Dunn, J. R., Domingues, C. M., & Wijffels, S. E. (2011). Pressure sensor drifts in Argo and their impacts, *Journal of Atmospheric and Oceanic Technology*, *28*, 1036–1049, doi:10.1175/2011JTECHO831.1.

Bellenger, H., & Duvel, J.-P. (2009). An analysis of tropical ocean diurnal warm layers, *Journal of Climate*, *22*, 3629–3646.

549 Carse, F., Buck, J., & Turton, J. (2012). Near-surface temperature profiles from pumped and un-
550 pumped Argo measurements, poster presented at the *4th Argo Science Workshop*, Venice,
551 Italy, 27–29, Sep.

552 Castro, S. L., Wick, G. A., & Emery, W. J. (2012). Evaluation of the relative performance of sea
553 surface temperature measurements from different types of drifting and moored buoys using
554 satellite-derived reference products, *Journal of Geophysical Research*, *117*,
555 doi:10.1029/2011JC007472.

556 Clayson, C. A., & Bogdanoff, S. D. (2013). The effect of diurnal sea surface temperature
557 warming on climatological air-sea fluxes, *Journal of Climate*, in press.

558 Clayson, C. A., & Weitlich, D. (2007). Variability of tropical diurnal sea surface temperature,
559 *Journal of Climate*, *20*, 334–352.

560 Cornillon, P., & Stramma, L. (1985). The distribution of diurnal sea surface warming events in
561 the western Sargasso Sea, *Journal of Geophysical Research*, *90*, 11,811–11,815.

562 Danabasoglu, G., Large, W. G., Tribbia, J. J., Gent, P. R., & Briegleb, B. P. (2006). Diurnal
563 coupling in the tropical oceans of CCSM3, *Journal of Climate*, *19*, 2347–2365.

564 Deschamps, P. Y., & Frouin, R. (1984). Large diurnal heating of the sea surface observed by the
565 HCMM experiment, *Journal of Physical Oceanography*, *14*, 178–184.

566 Donlon, C., and Coauthors, (2007). The global ocean data assimilation experiment high-
567 resolution sea surface temperature pilot project. *Bulletin of the American Meteorological*
568 *Society*, *88*, 1197–1213.

569 Fairall, C. W., Bradley, E. F., Godfrey, J. S., Wick, G. A., Edson, J. B., & Young, G. S. (1996).
570 Cool-skin and warm-layer effects on sea surface temperature, *Journal of Geophysical*
571 *Research*, *101*, 1295–1308.

572 Filipiak, M. J., Merchant, C. J., Kettle, H., & LeBorgne, P. (2010). A statistical model for sea
573 surface diurnal warming driven by numerical weather prediction fluxes and winds, *Ocean*
574 *Science Discussions*, *7*, 1497–1532.

575 Flament, P., Firing, J., Sawyer, M., & Trefois, C. (1994). Amplitude and horizontal structure of a
576 large sea surface warming event during the Coastal Ocean Dynamics Experiment, *Journal of*
577 *Physical Oceanography*, *24*, 124–139.

578 Gentemann, C. L., Donlon, C. J., Stuart-Menteth, A. C., & Wentz, F. J. (2003). Diurnal signals in
579 satellite sea surface temperature measurements, *Geophysical Research Letters*, *30*, 1140,
580 doi:10.1029/2002GL016291.

581 Gentemann, C. L., Minnett, P. J., LeBorgne, P. & Merchant, C. J. (2008): Multi-satellite
582 measurements of large diurnal warming events, *Geophysical Research Letters*, *35*, L22602,
583 doi:10.1029/2008GL035730.

584 Gentemann, C., L., Minnett, P. J., & Ward, B. (2009). Profiles of ocean surface heating (POSH):
585 A new model of upper ocean diurnal warming, *Journal of Geophysical Research*, *114*,
586 C07017, doi:10.1029/2008JC004825.

587 Ham, Y.-G., Kug, J.-S., Kang, I.-S., Jin, F.-F., & Timmermann, A. (2010): Impact of diurnal
588 atmosphere-ocean coupling on tropical climate simulations using a coupled GCM, *Climate*
589 *Dyn*amics, *34*, doi:10.1007/s00382-009-0586-8.

590 Horrocks, L. A., Harris, A. R., & Saunders, R. W. (2003). Modeling the diurnal thermocline for
591 daytime bulk SST from AATSR, *Technical Report FR 418*, U. K. Met Office, Exeter, United
592 Kingdom.

593 Johnson, G. C., Toole, J. M. & Larson, N. G. (2007). Sensor corrections for Sea-Bird SBE-41CP
594 and SBE-41 CTDs, *Journal of Atmospheric and Oceanic Technology*, *24*, 1117–1130,
595 doi:10.1175/JTECH2016.1.

596 Kawai, Y., & Kawamura, H. (2003). Validation of daily amplitude of sea surface temperature
597 evaluated with a parametric model using satellite data, *Journal of Oceanography*, *59*, 637–
598 644.

599 Le Borgne, Roquet, P., & Merchant, C. J. (2011). Estimation of sea surface temperature from the
600 Spinning Enhanced Visible and Infrared Imager, improved using numerical weather
601 prediction, *Remote Sensing of Environment*, *115*, 55–65.

602 Le Borgne, P., Legendre, G., & Péré, S. (2012). Comparison of MSG/SEVIRI and drifting buoy
603 derived diurnal warming estimates, *Remote Sensing of Environment*, *124*, 622–626.

604 Masson, S., Terray, P., Madec, G., Luo, J.-J., Yamagata, T., & Takahashi, K. (2011). Impact of
605 intra-daily SST variability on ENSO characteristics in a coupled model, *Climate Dyn*amics,
606 doi:10.1007/s00382-011-1247-2.

607 Pimentel, S., Haines, K., & Nichols, N. K. (2008). Modeling the diurnal variability of sea surface
608 temperatures, *Journal of Geophysical Research*, *113*, C11004, doi:10.1029/2007JC004607.

609 Ramp, S. R., Garwood, R. W., Davis, C. O., & Snow, R. L. (1991). Surface heating and
610 patchiness in the coastal ocean off Central California during a wind relaxation event, *Journal*
611 *of Geophysical Research*, *96*, 14,947–14,957.

612 Roemmich, D., et al. (2001). Argo: The global array of profiling floats, in *Observing the Oceans*
613 *in the 21st Century*, edited by C. J. Koblinsky and N. R. Smith, pp. 248–258, GODAE Project
614 Office, Melbourne, Victoria, Australia.

615 Saunders, P. M. (1967). The temperature at the air-sea interface, *Journal of Atmospheric*
616 *Sciences*, *24*, 269–273.

617 Schiller, A., & Godfrey, J. S. (2005). A diagnostic model for the diurnal cycle of sea surface
618 temperature for use in coupled ocean-atmosphere models, *Journal of Geophysical Research*,
619 110 C11014, doi:10.1029/2005JC002975.

620 Stramma, L., Cornillon, P., Weller, R. A., Price, J. F., & Briscoe, M. G. (1986). Large diurnal
621 sea surface temperature variability: Satellite and in situ measurements, *Journal of Physical*
622 *Oceanography*, *56*, 345–358.

623 Stuart-Menteth, A. C., Robinson, I. S., & Challenor, P. G. (2003). A global study of diurnal
624 warming using satellite-derived sea surface temperature, *Journal of Geophysical Research*,
625 *108*, 3155, doi:10.1029/2002JC001534.

626 Stuart-Menteth, A. C., Robinson, I. S., & Donlon, C. J. (2005). Sensitivity of the diurnal warm
627 layer to meteorological fluctuations. Part 2: A new paramterisation for diurnal warming,
628 *Journal of Atmospheric and Ocean Science*, *10*, 209–234.

629 Walton, C. C., Pichel, W. G., Sapper, J. F., & May, D. A. (1998). The development and
630 operational application of nonlinear algorithms for the measurement of sea surface
631 temperatures with the NOAA polar-orbiting environmental satellites, *Journal of Geophysical*
632 *Research*, *103*, 27,999–28,012.

633 Webster, P. J., Clayson, C. A., & Curry, J. A. (1996). Clouds, radiation, and the diurnal cycle of
634 sea surface temperature in the tropical western Pacific, *Journal of Climate*, *9*, 1712–1730.

635 Wick, G. A., Bates, J. J., & Scott, D. J. (2002). Satellite and skin-layer effects on the accuracy of
636 sea surface temperature measurements from the GOES satellites, *Journal of Atmospheric and*
637 *Oceanic Technology*, *19*, 1834–1848.

638 Woolnough, F., Vitart, S. J., & Balmaseda, M. A. (2007). The role of the ocean in the Madden-
639 Julian Oscillation: Implications for MJO prediction, *Quarterly Journal of the Royal*
640 *Meteorological Society*, *133*, 117–128.

641 Yu, F., Wu, X., Raja, M., Li, Y., Wang, L. & Goldberg, M. (2013). Diurnal and scan angle
642 variations in the calibration of GOES imager infrared channels, *IEEE Transactions on*
643 *Geoscience and Remote Sensing*, *51*, 671–683.

644 Zeng, X. & Beljaars, A. (2005). A prognostic scheme of sea surface skin temperature for
645 modeling and data assimilation, *Geophysical Research Letters*, *25*, 1411–1414.

646

647

Tables

Table 1. Statistics (number of matches, bias, and standard deviation (Stdev)) for the derived subskin and foundation temperature estimates from SEVIRI and Argo. Bias and standard deviation are given in K.

SST	Subskin					Foundation				
Profile Type	Argo No. Matches	Unpumped SEVIRI – Argo		Pumped SEVIRI–Argo		Argo No. Matches	Unpumped SEVIRI – Argo		Pumped SEVIRI – Argo	
		Bias	Stdev	Bias	Stdev		Bias	Stdev	Bias	Stdev
Warming	223	-0.04	0.39	0.23	0.44	211	-0.02	0.36	-0.16	0.36
Isothermal	405	-0.10	0.37	-0.09	0.35	495	-0.11	0.39	-0.10	0.38
All	628	-0.08	0.38	0.03	0.42	706	-0.09	0.38	-0.12	0.37

Table 2. Statistics for the derived DW estimates from SEVIRI and Argo and their corresponding differences.

Profile Type	No. matches	DW from SEVIRI		DW from Argo		ΔDW (SEVIRI – Argo)	
		Mean (K)	Stdev (K)	Mean (K)	Stdev (K)	Bias (K)	Stdev (K)
Warming	192	0.40	0.36	0.40	0.36	0.00	0.25
Isothermal	317	0.02	0.17	0.00	0.00	0.02	0.17
All	509	0.16	0.32	0.15	0.29	0.01	0.21

Table 3. Statistics for the residual difference in derived DW estimates showing warming stratified by percentage of clear sky pixels in the SEVIRI 5x5 imagettes.

% Clear Sky Pixels	ΔDW Warm			ΔDW Isothermal			ΔDW All		
	No. Matches	Bias (K)	Std. Dev. (K)	No. Matches	Bias (K)	Std. Dev. (K)	No. Matches	Bias (K)	Std. Dev. (K)
20	33	-0.01	0.28	109	-0.00	0.20	142	-0.01	0.22
40	18	-0.01	0.15	42	0.03	0.15	60	0.02	0.15
60	24	0.03	0.28	49	-0.01	0.17	73	0.01	0.21
80	33	0.01	0.23	32	0.08	0.14	65	0.04	0.19
100	84	0.00	0.26	85	0.03	0.16	169	0.01	0.21
ALL	192	0.00	0.25	318	0.02	0.17	509	0.01	0.21

Figure Captions

Figure 1. Example of an unpumped APEX Argo NST profile (black) showing a diurnal thermocline in the top 5 dbar. Blue and red asterisks illustrate the location of the extracted foundation and subskin SST estimates from the profile, respectively. The circles illustrate the corresponding foundation and subskin estimates extracted from SEVIRI.

Figure 2. Example of the SEVIRI foundation SST estimate for (a) a single day (January 28, 2012), and (b) the climatological average, between 2009–2012, of the SEVIRI foundation temperatures for the corresponding month of January.

Figure 3. Location of Argo and SEVIRI collocations grouped by season. The background images correspond to the peak diurnal warming amplitude for the season over the 3-years of the study. Cases with observed diurnal warming in the Argo profiles are indicated with the magenta symbols, while the isothermal profiles are indicated with black.

Figure 4. Scatterplots comparing the derived (a) subskin and (b) foundation temperature estimates from SEVIRI and the unpumped Argo data. The red symbols correspond to the cases where diurnal warming was observed in the Argo profiles, while the black symbols represent the isothermal cases. The corresponding statistics are included in Table 1.

Figure 5. Comparison of derived DW estimates from SEVIRI and unpumped Argo data. The corresponding statistics are included in Table 2.

Figure 6. Scatterplot illustrating the high level of correlation between differences in the subskin and foundation temperature estimates from SEVIRI and Argo. The red symbols correspond to the cases where diurnal warming was observed in the Argo profiles while the black symbols represent the isothermal cases. The Pearson correlation coefficient for all points combined is 0.84 as noted.

Figure 7. Percentage of cloud coverage in the derived SEVIRI foundation temperature over the period from 2009 – 2012.

Figure 8. Dependence of the residual difference in the DW estimates from SEVIRI and Argo on (a) the SEVIRI – Argo subskin SST difference, and (b) the SEVIRI – Argo foundation temperature difference.

Figures

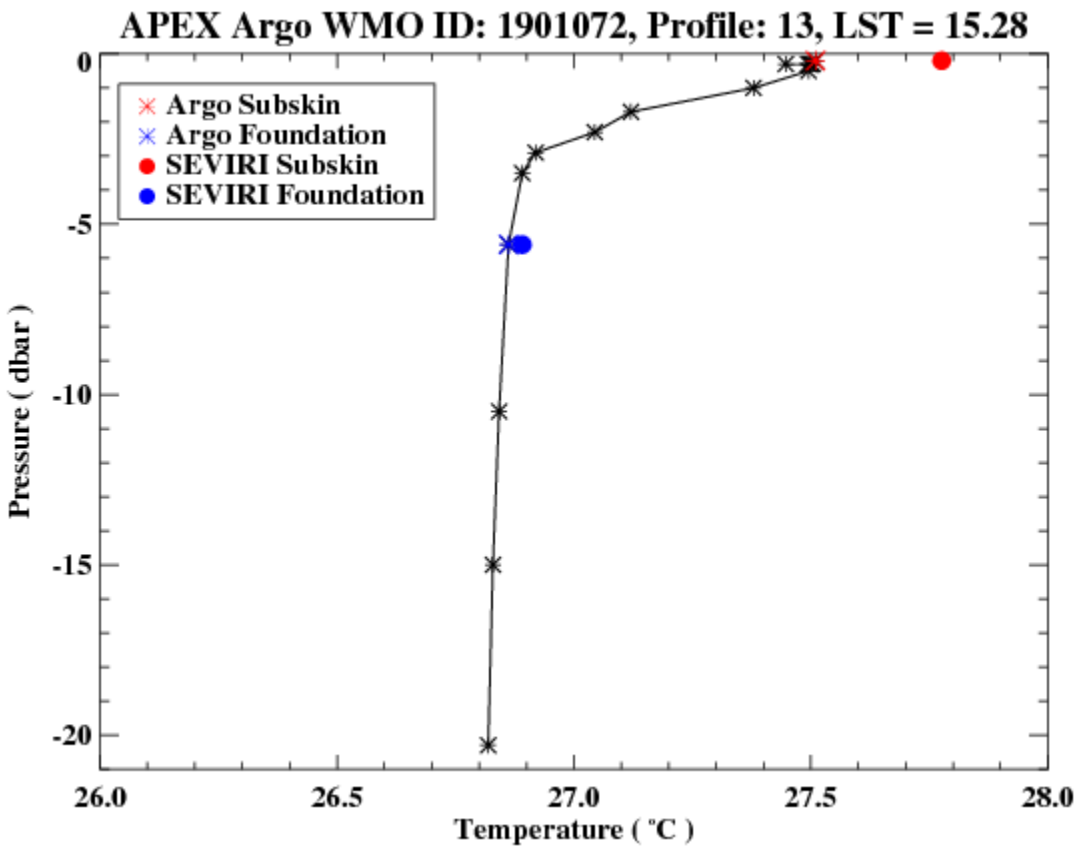

Figure 1. Example of an unpumped APEX Argo NST profile (black) showing a diurnal thermocline in the top 5 dbar. Blue and red asterisks illustrate the location of the extracted foundation and subskin SST estimates from the profile, respectively. The circles illustrate the corresponding foundation and subskin estimates extracted from SEVIRI.

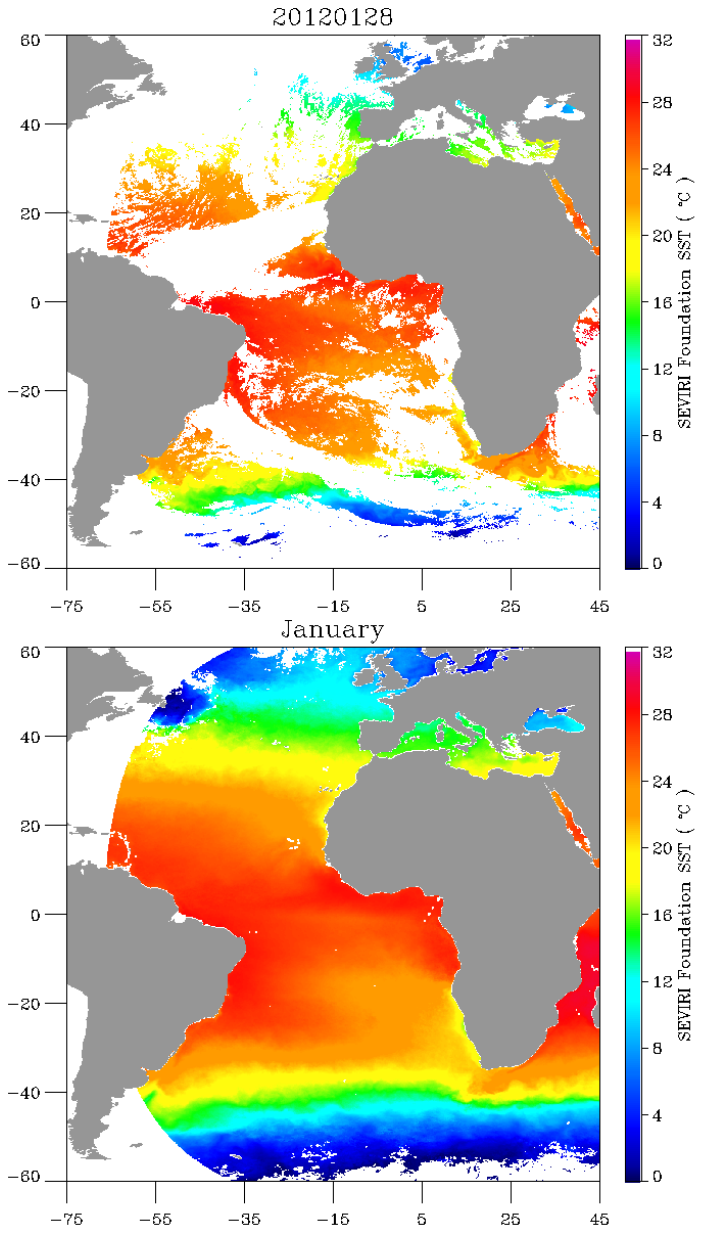

Figure 2. Example of the SEVIRI foundation SST estimate for (a) a single day (January 28, 2012), and (b) the climatological average, between 2009–2012, of the SEVIRI foundation temperatures for the corresponding month of January.

719

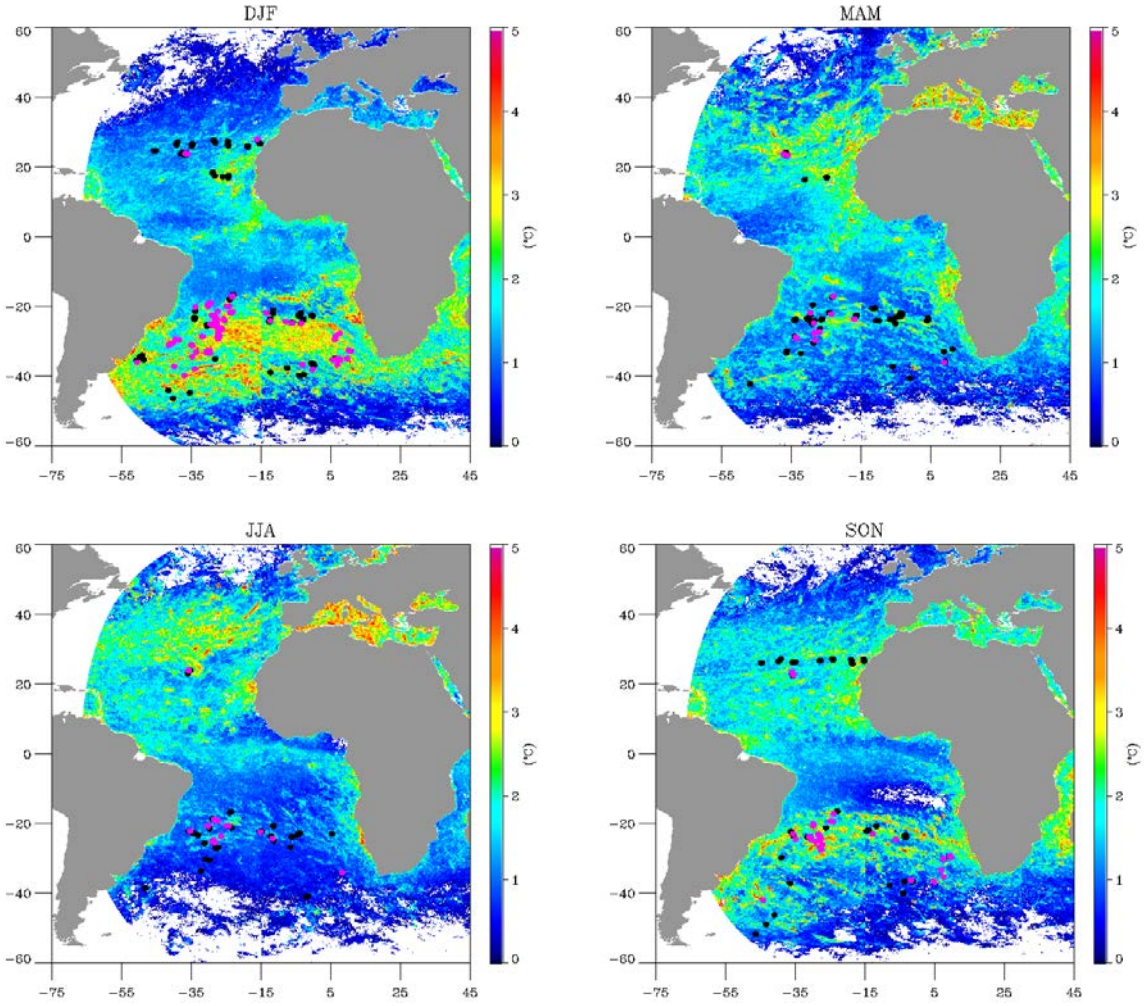

720

721 **Figure 3.** Location of Argo and SEVIRI collocations grouped by season. The background
722 images correspond to the peak diurnal warming amplitude for the season over the 3-years of the
723 study. Cases with observed diurnal warming in the Argo profiles are indicated with the magenta
724 symbols, while the isothermal profiles are indicated with black.

725

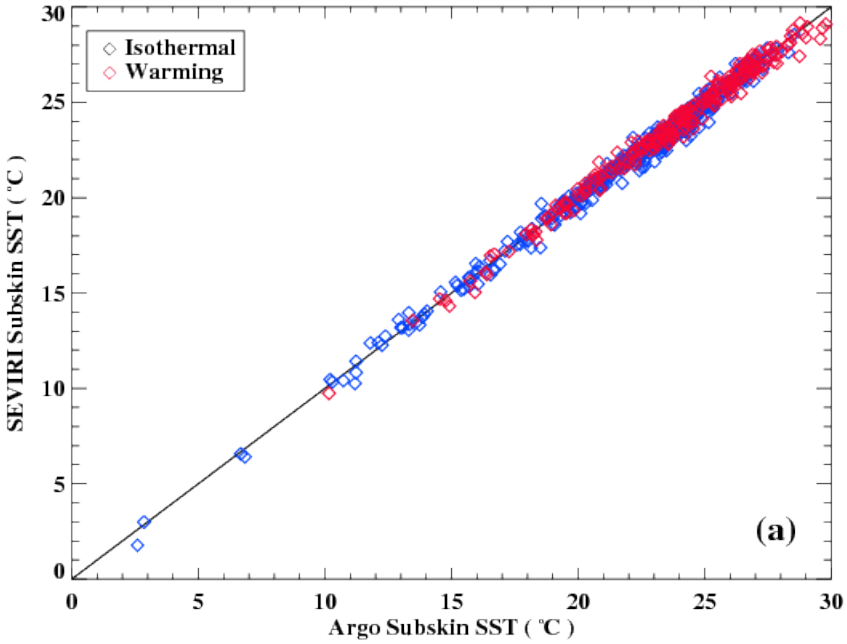

726

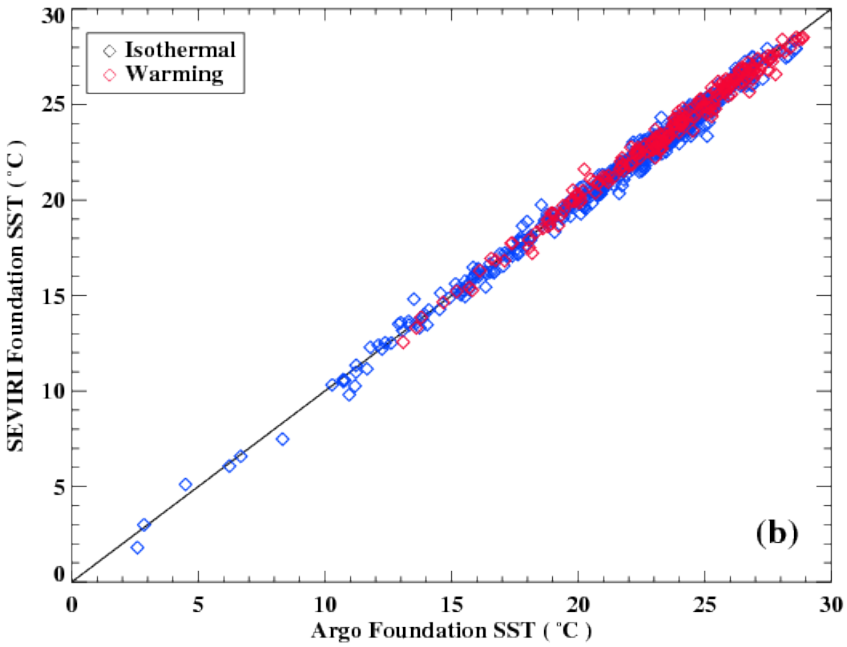

727

728 **Figure 4.** Scatterplots comparing the derived (a) subskin and (b) foundation temperature
729 estimates from SEVIRI and the unpumped Argo data. The red symbols correspond to the cases
730 where diurnal warming was observed in the Argo profiles, while the black symbols represent the
731 isothermal cases. The corresponding statistics are included in Table 1.

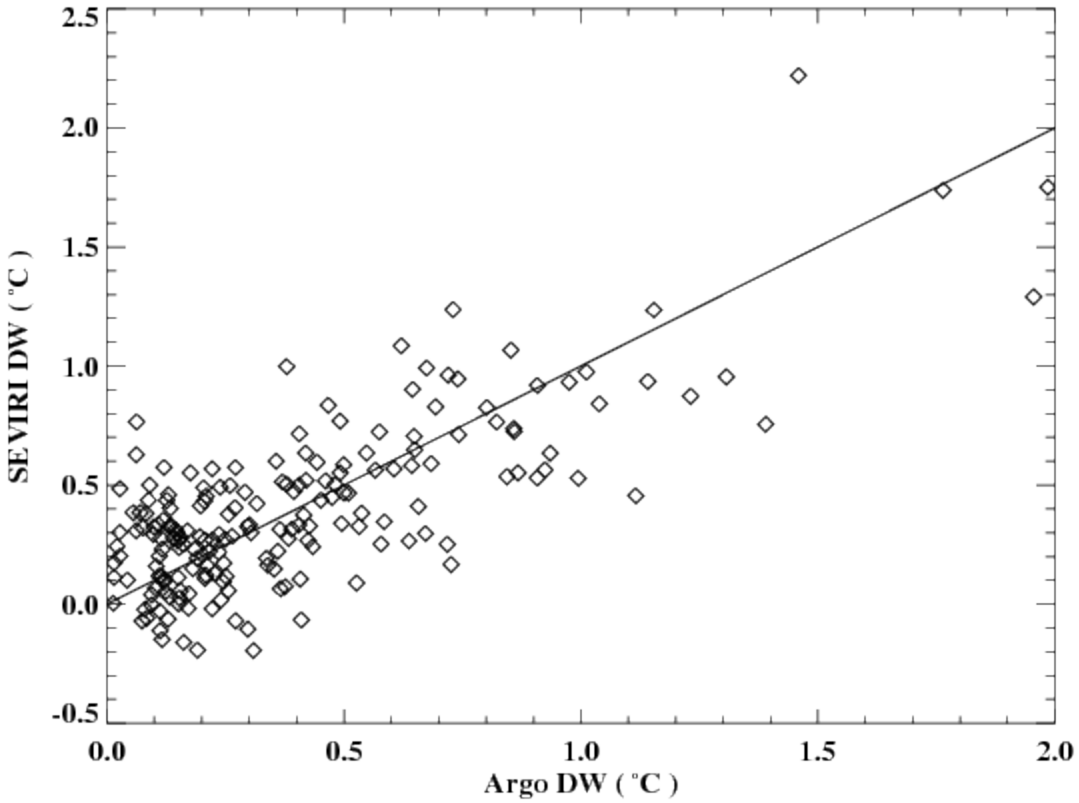

732

733 **Figure 5**. Comparison of derived DW estimates from SEVIRI and unpumped Argo data. The

734 corresponding statistics are included in Table 2.

735

736

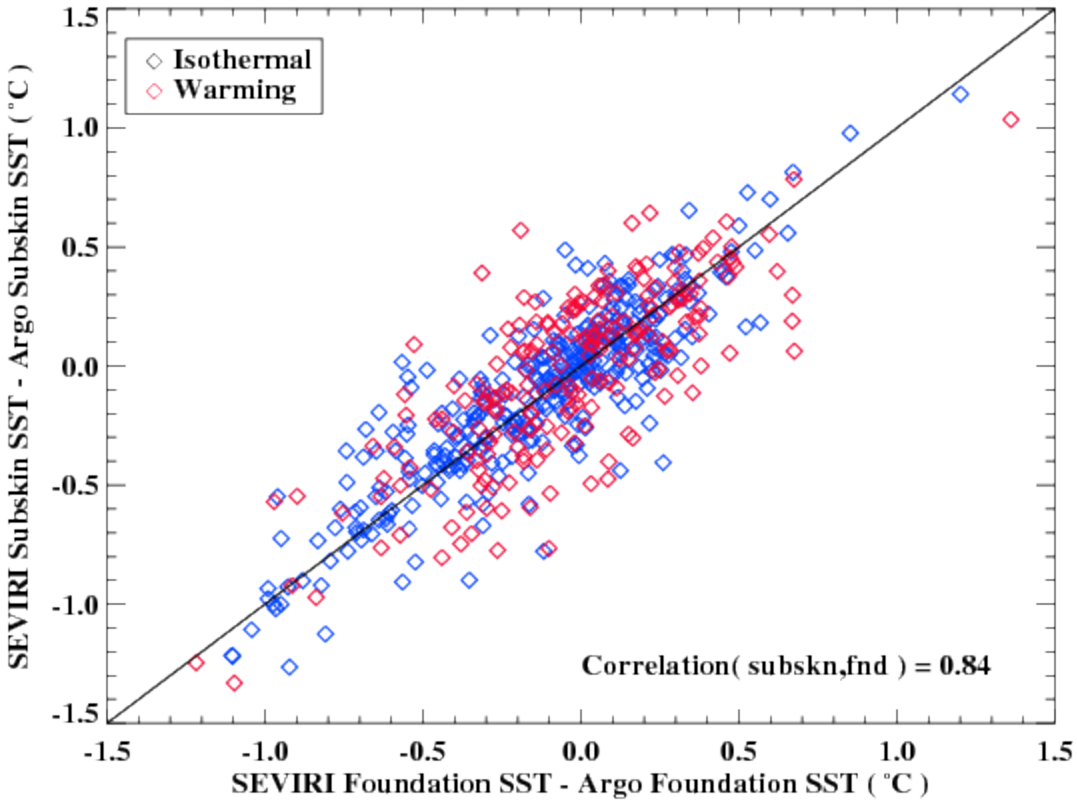

737

738 **Figure 6.** Scatterplot illustrating the high level of correlation between differences in the subskin
739 and foundation temperature estimates from SEVIRI and Argo. The red symbols correspond to
740 the cases where diurnal warming was observed in the Argo profiles while the black symbols
741 represent the isothermal cases. The Pearson correlation coefficient for all points combined is
742 0.84 as noted.

743

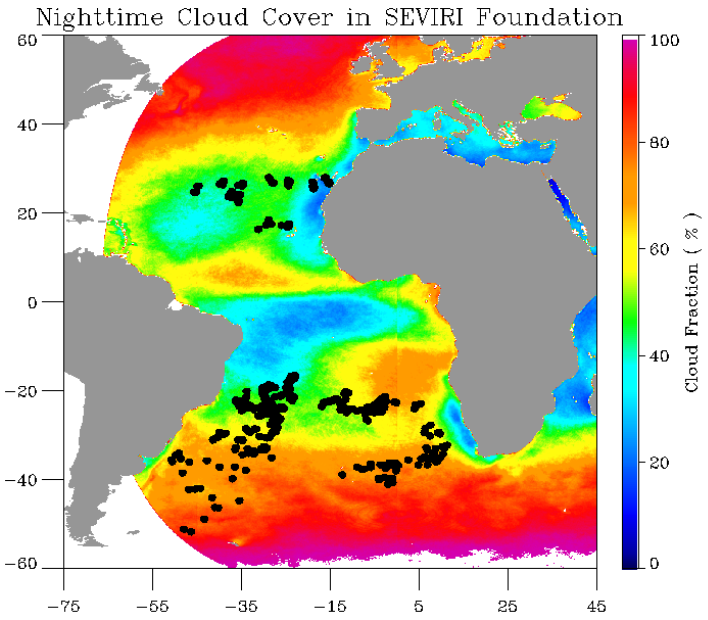

744

745 **Figure 7.** Percentage of cloud coverage in the derived SEVIRI foundation temperature over the

746 period from 2009 – 2012.

747

748

749

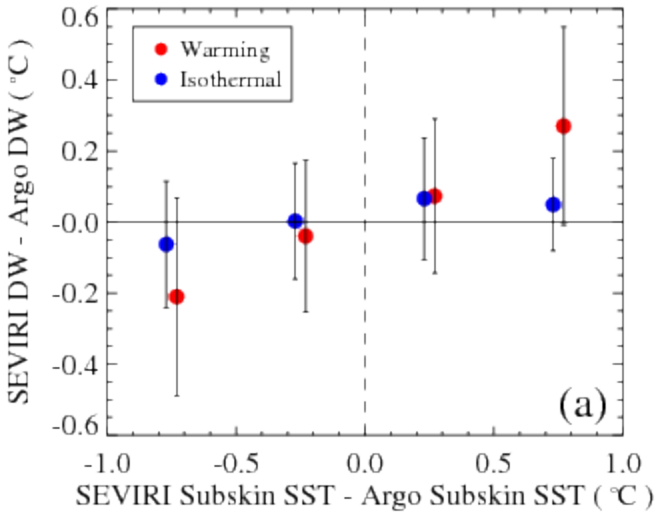

750

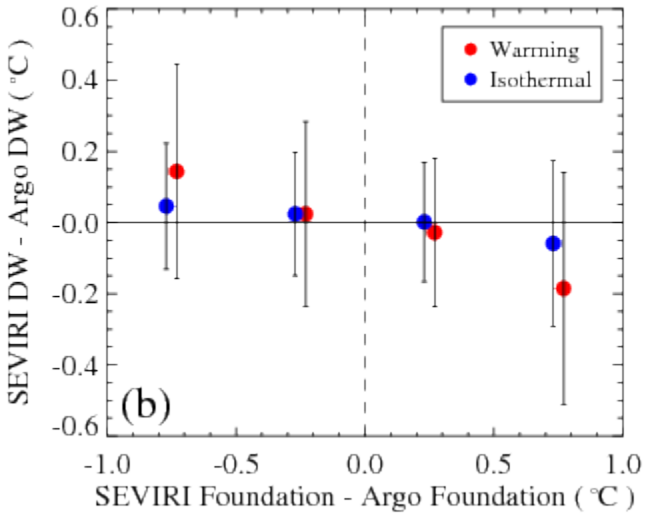

751

752 **Figure 8.** Dependence of the residual difference in the DW estimates from SEVIRI and Argo on

753 (a) the SEVIRI – Argo subskin SST difference, and (b) the SEVIRI – Argo foundation

754 temperature difference.